

# We are IntechOpen, the world's leading publisher of Open Access books Built by scientists, for scientists

6,900

Open access books available

185,000

International authors and editors

200M

Downloads

Our authors are among the

154

Countries delivered to

TOP 1%

most cited scientists

12.2%

Contributors from top 500 universities



WEB OF SCIENCE™

Selection of our books indexed in the Book Citation Index  
in Web of Science™ Core Collection (BKCI)

Interested in publishing with us?  
Contact [book.department@intechopen.com](mailto:book.department@intechopen.com)

Numbers displayed above are based on latest data collected.  
For more information visit [www.intechopen.com](http://www.intechopen.com)



# Luminescent Materials in Lighting, Display, Solar Cell, Sensing, and Biomedical Applications

*Abhishek Kumar Soni and Bheeshma Pratap Singh*

## Abstract

This chapter comprises a broader extent of the luminescence phenomenon with the mechanism involved therein as well as applications. Typically, the up and down conversion and downshifting behavior of the optical materials have been elucidated in brief. The fundamental understanding of these optical materials has been described by using schematic representations. It is well documented that the rare earth-based optical materials are known for their luminescent enrichment due to availability of the ladder-like energy levels. These energy levels can be utilized for the excitation of the luminescent materials by using a suitable excitation source. In the process of development of luminescent materials, choice of host matrices and dopant ions is very crucial. Strong correlation of these optical materials has been shown with the current scenario of our society and daily life. In view of the ongoing research, nanophosphor, glasses, and quantum dots with size- and shape-dependent optical behavior have been given in detail. The involved mechanism and the energy transfer phenomenon have been well elucidated by schematic and figures for the evident explanation to the readers. Our emphasis is to elucidate these optical materials in the development of innovative multifunctional applications such as lighting, display, sensing, LEDs, solar cell, and biological applications.

**Keywords:** light conversion, phosphor, quantum dots, optical temperature sensing, LEDs, solar cell, biological and clinical

## 1. Introduction

### 1.1 Luminescence in rare earth ions

In 1888, German physicist Wiedemann for the very first time employed the term “luminescence.” Luminescence promotes emission of light from a material at a certain excitation wavelength. It can be categorized into diverse kinds depending upon the various involved processes of excitation. It is classified as photoluminescence, thermoluminescence, electroluminescence, and chemiluminescence. Photoluminescence is a process in which the emission of light (photon) can be obtained from the object upon excitation. It is subgrouped into fluorescence and phosphorescence. In the thermoluminescence phenomenon, emission of light from a solid material occurs upon heating. Electroluminescence arises from gases under applied electrical potentials, while chemiluminescence may prevail during

the chemical reaction process [1–3]. The fluorescence phenomenon exhibits a short time duration of decay levels, while phosphorescence exhibits prolonged decay time after the cease of the excitation source. Inorganic materials accommodated with impurity foreign ions most commonly lanthanide ions exhibiting luminescence upon excitation are known as phosphors.

In 1994, Bhargava et al. [4] reported for the very first time on  $\text{Mn}^{2+}$ -doped ZnS DCNCs that exhibit characteristic features such as change in band gap and shifting of emission and excitation spectra of prepared nanomaterials. An external quantum efficiency of up to 18% was observed. This report opened the new pathways in the field of nanophosphor research area.

Optical materials doped with lanthanide activators are very promising candidates for photoluminescence studies. The luminescent material exhibiting luminescence properties can be utilized for solid state lighting (SSL), light emitting diodes (LEDs), display devices, solar cell, sensing, and biomedical applications. The advantage of these luminescent materials in diverse application fetches among the researchers to search the novel improved materials with magnified luminescence properties. RE ions exhibit ladder-type energy levels and sharp emission lines. Upon doping into a low phonon frequency host lattice, these ions can be easily excited by employing different excitation sources.

Up-conversion is a non-linear anti-stokes optical process in which a low energy input photon is converted into a high energy output photon by the process of sequential multiphoton absorption. Surprisingly, due to different involved energy transfers in different RE ions, the emission properties can be manipulated by suitable doping and/or co-doping.

This chapter has been considered to account for basic understanding involved in the luminescent materials, viz. up- and down-conversion and downshifting behavior of the optical materials. These nanomaterials could be a reasonable alternative for novel multi-functional optical materials utilized in lighting, display, sensing, LED, solar cell, biological, and clinical applications. Quantum dots (QDs) and their uses in the biological and clinical application have been justified in view of current uses. **Figure 1** shows the various applications of luminescent materials.

## 1.2 Rare earth elements

Commonly known as 4f- block elements having an atomic number ranging from 57 (La) to 71 (Lu), these elements adjusted themselves at the bottom of the Mendeleev periodic table.

## 1.3 Silent features of the rare earth elements

The f-block elements reveal various well-defined features that distinguish them from the d-block metals. Some of the peculiar properties of f-block elements are as follows:

- i. The f-block elements manifest a range of coordination numbers (6–12).
- ii. RE ions form ionic complexes that undergo facile exchange of ligands.
- iii. RE ions reveal small and very sharp electronic spectra and less crystal-field splitting.
- iv. Since 4f orbitals in the RE ions are well shielded by  $5s^2$  and  $5p^6$  orbitals, therefore their optical properties are mostly not changed by the host.

v. RE ions most commonly exist in its 3+ stable oxidation state.

vi. Some RE elements also reveal other valence states such as 2+ and 4+ under specific conditions.

#### 1.4 Spectroscopy of rare earth elements

A partially filled 4f shell is well shielded from completely filled outer 5s<sup>2</sup> and 5p<sup>6</sup> orbitals which gives it sharp electronic spectra. The energy level spectra of REs do not alter to the outer environment in which they are indulged.

In general, lanthanide ions exist in 3+ state and also exhibit 2+ oxidation state in some case. RE ions in triplet states demonstrate intra-4f-4f transitions which thus result in an intense narrow emission band in a vast variety of host matrices. The shielding of 4f orbitals furnished by the 5s<sup>2</sup> and 5p<sup>6</sup> electrons promotes to radiative transitions which match well with the free ions. Some other RE ions such as Sm<sup>2+</sup> and Eu<sup>2+</sup> show the divalent character. These ions also reveal the visible luminescence under suitable excitation wavelength. Moreover, this book chapter is predominantly based on the luminescence of the trivalent RE ions.

Neutral RE elements reveal the electronic configuration [Xe] 4f<sup>N</sup>6s<sup>2</sup> or [Xe] 4f<sup>N-1</sup>5d 6s<sup>2</sup>, where [Xe] constitutes a xenon core whose electronic structure is represented as [Xe] = [1s<sup>2</sup>2s<sup>2</sup>2p<sup>6</sup>3s<sup>2</sup>3p<sup>6</sup>3d<sup>10</sup>4s<sup>2</sup>4p<sup>6</sup>4d<sup>10</sup>5s<sup>2</sup>5p<sup>6</sup>]. The electrostatic shielding of 4f orbitals by the outermost 5s<sup>2</sup>5p<sup>6</sup> orbitals leads an atom-like behavior in RE ions under a solid host matrix such as a crystal or glass.

Term and symbol is represented as <sup>(2S+1)</sup>L<sub>J</sub>, where S, L, and J are total multiplicity, orbital angular momentum and angular momentum, respectively. Involved selection rules for intra f-f transitions in lanthanide ions are given in **Table 1**.

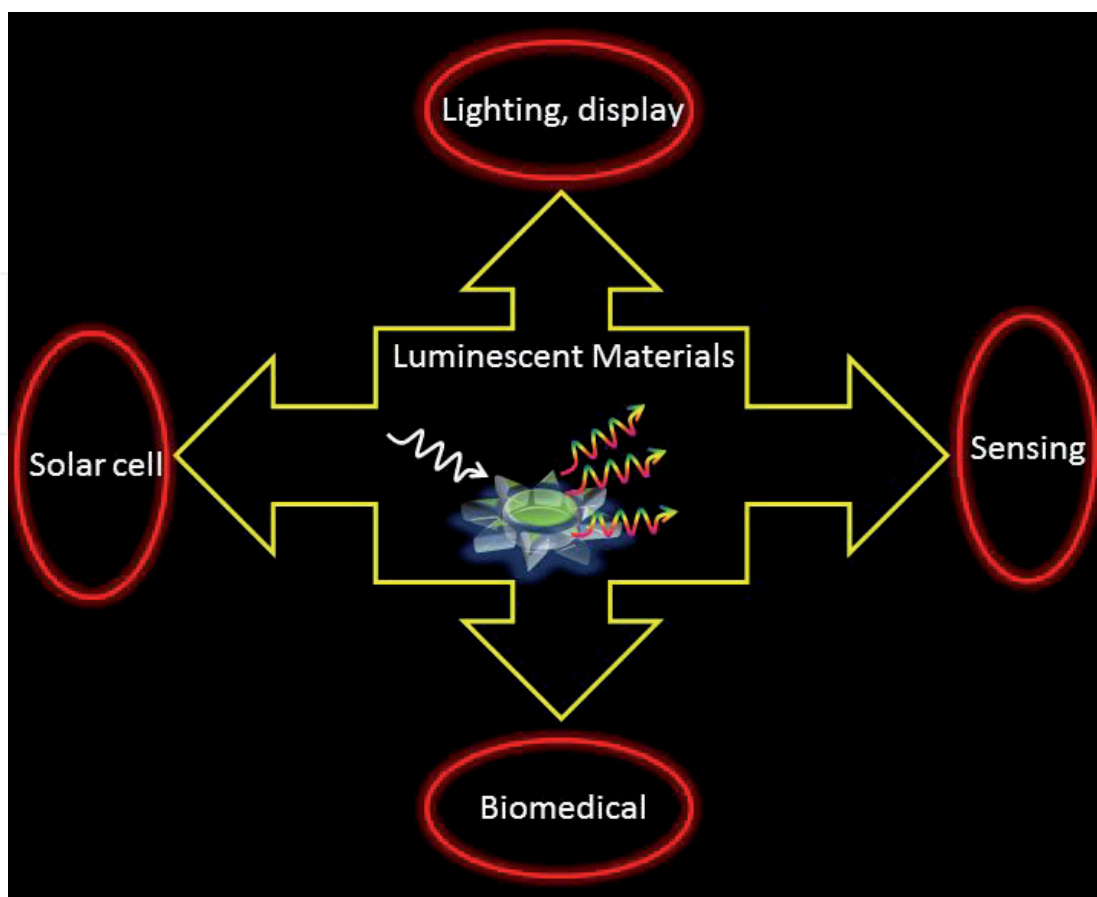


**Figure 1.**  
*Various applications of luminescent materials.*

Operator	Parity	$\Delta S$	$\Delta L$	$\Delta J^*$
Electric dipole	Opposite	0	$\leq 6$	$\leq 6$ (2, 4, 6, if J or J' = 0)
Magnetic dipole	Same	0	0	0, $\pm 1$
Electric quadrupole	Same	0	0, $\pm 1, \pm 2$	0, $\pm 1, \pm 2$

*\*J = 0 to J' = 0 transitions are forbidden always; J = 0  $\rightarrow$  J' = 1, 3, 5 exhibit weak transition intensity; and J = 0  $\rightarrow$  J' = 2, 4, 6 convey strong transition intensity.*

**Table 1.**  
Selection rules for intra f-f transitions in lanthanide ions.

### 1.5 Rare earth ion levels in solids

According to Laporte rule, 4f-4f transitions are forbidden and show a very weak oscillator strength of about  $\sim 10^{-6}$ .

The Hamiltonian of a particular RE ion can be represented as follows [5]:

$$H = H_{\text{free ion}} + V_{\text{Host}} + V_{\text{EM}} + V_{\text{Vib.}} + V_{\text{ion-ion}} \quad (1)$$

where  $H_{\text{free ion}}$  represents the Hamiltonian of an isolated ion,  $V_{\text{Host}}$  describes the environment effect on the RE ion,  $V_{\text{EM}}$  describes RE ion with an electromagnetic field interaction,  $V_{\text{Vib}}$  describes the interaction of RE ion with host lattice vibrations, and  $V_{\text{ion-ion}}$  describes the interaction between the RE ions, respectively. The Hamiltonian of free ion ( $H_{\text{free ion}}$ ) can be splitted into several components, i.e.,

$$H_{\text{free ion}} = H_{\text{CF}} + H_{\text{C}} + H_{\text{SO}} \quad (2)$$

where  $H_{\text{CF}}$  belongs to central-field Hamiltonian which reveals the interaction of an orbiting electron with the nucleus and effective field from all other electrons, while  $H_{\text{C}}$  term represents the residual Columbic interaction of the 4f electrons with each other when there is no centrally symmetric contribution and  $H_{\text{SO}}$  is the spin-orbit coupling, respectively.

### 1.6 Suitable hosts for doping of rare earth ions

For efficient device applications, a lanthanide-based activator as a foreign ion and selection of a good host matrix are of vital importance. Energy level structures of most of the lanthanide ions are independent of the host matrices but phonon frequency plays an important role in nonradiative transitions via multi-phonon relaxation between closely spaced energy levels. The nonradiative relaxation rate can be evaluated by the energy gap law [6],

$$k_{\text{nr}} = \beta_{\text{el}} \exp(-\alpha(\Delta E - 2\hbar\omega_{\text{max}})) \quad (3)$$

where " $\beta_{\text{el}}$ " and " $\alpha$ " are constants for a given host lattice, " $\Delta E$ " is the energy difference between the energy levels under consideration, and  $\hbar\omega_{\text{max}}$  is the maximum phonon energy of the host. Hosts having low phonon energy decrease the possibility of nonradiative relaxation channel rate, which promotes to high luminescence efficiency. The phonon frequencies of some host matrices are listed in **Table 2**.

Host matrices	Phonon frequency ( $\sim\text{cm}^{-1}$ )
Borate	1400
Phosphate	1100
Silicate	1000–1100
Germanate	800–975
CaMoO <sub>4</sub>	800
Tellurite	600–850
YVO <sub>4</sub>	600
Fluoride	500–600
LaCl <sub>3</sub>	260
Bromide	175–190
LaBr <sub>3</sub>	175
Iodide	160

**Table 2.**  
*Host matrices with maximum phonon frequency for different hosts [7].*

## 2. Mechanism: down-conversion and up-conversion processes

### 2.1 Energy transfer in down conversion process

The downshifting process is a single photon process in which a high energy absorbed photon is converted into a low energy photon. This process is governed by the Stokes law. Luminescence of an optical material is ruled by the energy transfer process involved between acceptor and donor ions. Mostly, resonant radiative energy transfer, nonradiative energy transfer, and phonon assisted energy transfer between donor (D) and acceptor (A) are prominent energy transfer processes involved in the lanthanide ions. These important processes are represented in **Figure 2**.

### 2.2 Energy transfer in up-conversion

In 1960, Auzel has first observed the up-conversion (UC) phenomenon. It is a nonlinear anti-Stokes process in which two or more than two lower energy input pumped photons are converted into a high energy output photon [8]. There are some more different types of processes involved in the UC phenomenon. The more common energy transfer processes involved in the UC process are described as follows:

#### 1. Ground state absorption (GSA)

The RE ion lying in the ground state absorbs the excitation energy and gets promoted to a higher excited level. This process involves the single ion.

#### 2. Excited state absorption (ESA)

The atom in the excited level will be further promoted to the higher levels upon excitation. The ions from the higher level upon de-excitation emit an up-converted photon. This is also a single-ion process.

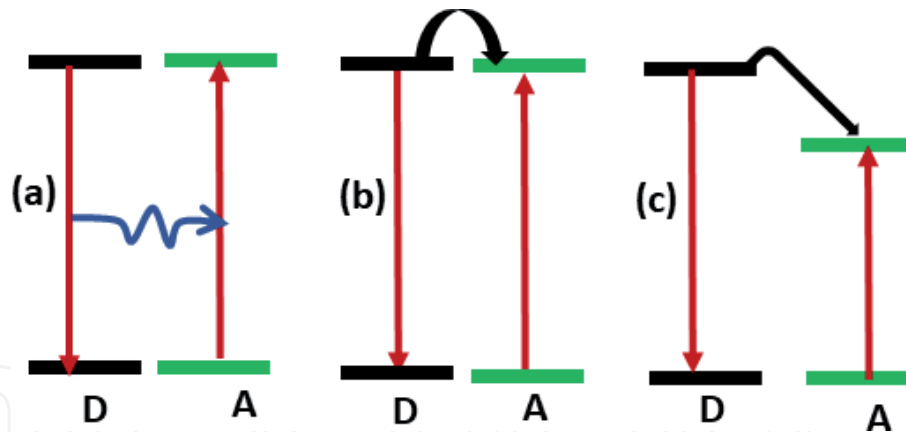


**Figure 2.** (a) Resonant radiative energy transfer, (b) nonradiative energy transfer, and (c) phonon assisted energy transfer between donor (D) and acceptor (A) ions.

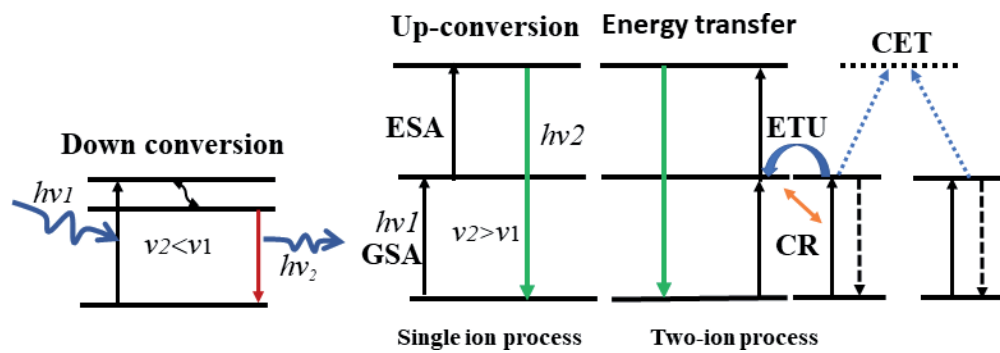


**Figure 3.** Schematics of various processes, viz. down-conversion, up-conversion, and involved energy transfers.

### 3. Energy transfer up-conversion (ETU)

It is governed by participation of two different adjacent ions in which one ion acts as a sensitizer and absorbs the excitation energy, which is transferred to the neighboring ion acting as an activator (already lying in the excited state). The emitted photon can have higher energy excited photon.

### 4. Cross-relaxation process (CR)

If two sets of energy levels (in the same ion or in two different ions) are having the same energy difference between them, then there is certain probability of energy transfer and/or exchange occurring between the levels under consideration.

### 5. Co-operative energy transfer (CET)

When two active ions in a metastable intermediate level interact with each other and excite one ion into a high lying level and the other ion getting de-excited, in this process, very high concentration of doping is required.

The abovementioned energy transfer processes have been summarized in **Figure 3**.

## 3. Applications of the luminescent materials

### 3.1 Lanthanide doped nanophosphor materials as a solar spectral convertor for photovoltaic applications

There is tremendous research and advancement going on in the field of solar cell technology. It is still a challenging task for the photovoltaic (PV) community

to prepare highly efficient and cost-effective conversion of solar energy into electricity. The spectral distribution of Sun light at Air Mass 1.5 global (AM 1.5G) constitutes with the photons having wide spectral range varying from ultraviolet to infrared (200–2500 nm) since PV cells are only sensitive to a small fraction of the incident solar photons. This is due to the fact that current solar materials respond to a narrow range of solar photons. Photons having energy higher than the bandgap of the material are only absorbed and excess energy is released in the form of heat [9].

In order to utilize the whole solar spectrum, a novel perspective through use of up and down conversion and quantum cutting has been exploited as an optical material that can act as a spectral converter since lanthanide-doped nanophosphor materials reduce the spectral mismatch losses, and therefore magnify the efficiency of photovoltaics.

In the up-conversion process, the sub-band gap of solar spectra is utilized. It is reported for  $\text{Tm}^{3+}$ ,  $\text{Er}^{3+}$ , and  $\text{Ho}^{3+}$  co-doped with  $\text{Yb}^{3+}$  up-converters for wide band gap solar cells, while  $\text{Er}^{3+}$  doped up converters for c-Si solar cells. Moreover,  $\text{Ln}^{3+}$  doped up-convertors are under study for solar cells and have low conversion efficiency (~3%). The up-conversion efficiency may be magnified by employing plasmon resonance, quantum dots, and organic dyes [10–12].

Quantum cutting permits the effective use of the high energy photons which have above band gap value, which furnishes potential for efficiency enhancement of narrow band gap solar cells such as c-Si solar cells. An internal quantum efficiency of ~200% has been reported in lanthanide ( $\text{Ln}^{3+} = \text{Tb}, \text{Er}, \text{Pr}, \text{Tm}, \text{Dy}, \text{Nd}, \text{and Ho}$ ) coupled with  $\text{Yb}^{3+}$  for narrow band c-Si solar cells [10].

$\text{Yb}^{3+}$  ions act as an acceptor with NIR emission band at ~980 nm which has a band gap just above the band gap of c-Si. In order to improve the absorption cross-section which is common in lanthanide activators, other ions such as  $\text{Ce}^{3+}$ ,  $\text{Eu}^{2+}$ ,  $\text{Yb}^{3+}$ , and  $\text{Bi}^{3+}$  ions and/or hosts have been utilized for sensitization purpose [13–15]. The up-conversion-based material is kept in between a bifacial solar cell reflecting layer which is utilized to harvest the sub-bandgap of solar spectrum. The quantum cutting phenomenon is a linear process which is independent of the incident power. This permits the use of nonconcentrated sunlight [16]. Quantum-cutting-based optical materials are adjusted on the front surface of a mono-facial solar cell which permits the absorption of down converted photons by the solar cell.

Downshifting furnishes the accomplishment to enhance the spectral response of solar cells into short-wavelength regime. In order to enhance power-conversion efficiency in solar cells, RE-doped phosphors and glasses, QDs, and lanthanide-based organic complexes can be employed as solar concentrators and downshifting layers. Spectral conversion modules involving down-shifting (DS), quantum-cutting (QC), and up conversion (UC) materials for PV applications have been shown in **Figure 4** [10].

### 3.2 Quantum dots

In case of quantum dots (QDs), particle size is squeezed below its Bohr radius, which is termed as the quantum confinement effect. Under the quantum confinement effect, color of the QDs can be manipulated according to size and composition. It is due to the quantum confinement effect, emission color of QDs can be managed according to their size and composition [17]. Owing to these characteristics, QDs are applicable in solar cells, lasers, bio-imaging, and light-emitting diodes (LEDs) [18–21]. QDs can be mainly classified into Cd-based QDs as CdSe, CdTe and PbS, Cd-free InP,  $\text{CuInS}_2$ , and all inorganic  $\text{CsPbBr}_3$  and mixed halide and  $\text{CH}_3\text{NH}_3\text{PbBr}_3$  perovskite quantum dots (PQDs) [22–26]. PQDs comprise  $\text{ABX}_3$  compositional formula unit in which A represents cesium (Cs), methyl ammonium

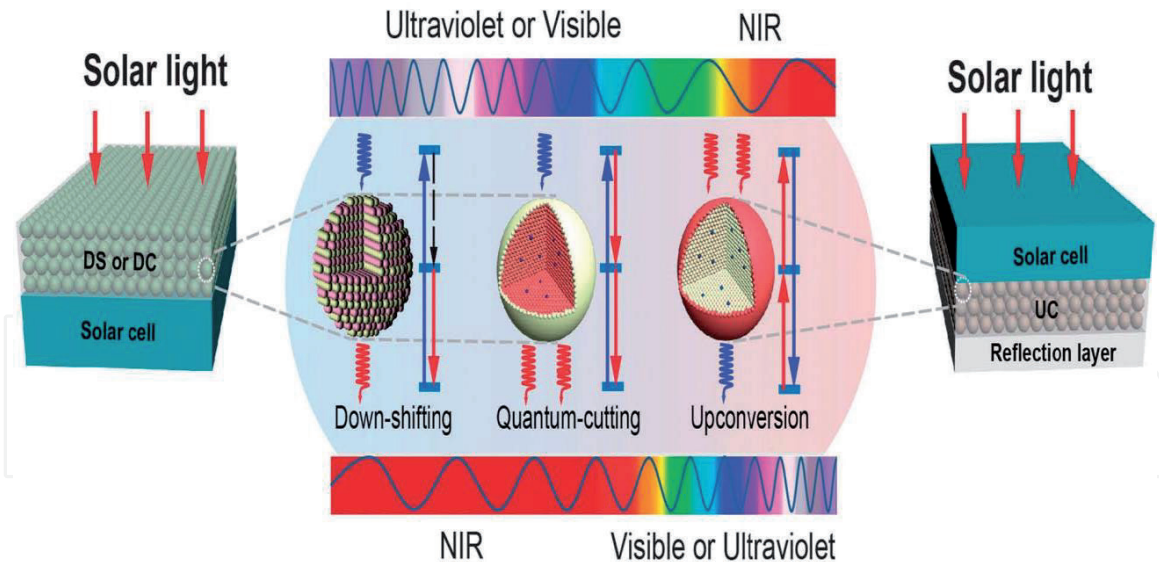


**Figure 4.** Schematic spectral conversion module for photovoltaic utility involving down-shifting, quantum-cutting, and up-conversion-based luminescent materials. Reproduced with permission from reference [10].

(MA), while B represents Pb and/or Sn cations, and X represents Cl, Br, and/or I, that is, halide anions. QD-based LEDs with narrow FWHM can improve LED conversion efficiency from 5% to 15% and have correlated color temperature (CCT) values in the range of 5000–2700 K as compared to commercial red phosphor-based LEDs [27].

QLED devices gained curiosity in recent years over organic light-emitting diodes (OLEDs) due to their high color purity, relatively less cost, and lower energy consumption. The color gamut value for highly efficient QLEDs surpass 140% of the NTSC standard higher than that of commercial OLED. QD-based W-LEDs can reach ~104% enhancement of the NTSC standard [28]. High color purity of QLED devices annihilates the use of color filters, which magnify the power consumption value. QLED-based device performance is influenced by several constituents such as photoluminescence quantum yield (PLQY) of QD films, electron-hole pair efficiency from transport layer, and band arrangement of the device. A Cd-based red QLED device has been reported having ~20% external quantum efficiency (EQE) which is comparable to that of commercial OLEDs [29].

Instant development perspective for the first to fifth generations of white-light LED (W-LED) and lighting devices has been shown by Yoon et al. [30]. The very first generation of W-LED is mainly based on InGaN blue chip incorporated with yellow-emitting phosphors (YAG:Ce). Moreover, red color component of YAG-Ce-based W-LEDs is very feeble and it attains cool white light having a CRI value of ~70–80 [31, 32]. In order to enhance CRI values, in the 2nd generation, red emitting nitride phosphor-based LEDs are developed. Moreover, employed red nitride materials reveal lower efficiency since they possess a broader full width at half maximum (FWHM) and inherent subsidiary scattering loss. In the third generation, W-LEDs can be transformed as advanced in the form of backlight display. Red-QDs and narrow-band phosphor (KSF) are employed for the high-quality display applications. Prepared devices revealed wide color gamut as compared to traditional phosphor device. Red-QDs combined with YAG phosphor produce warm W-LEDs having a higher CRI value [33]. Wang et al. [34] incorporated red color CdS-ZnS: Cu QDs incorporated with YAG:Ce. In this study, the obtained device showed high values of CRI ( $R_a = 90$ ) and CCT (4927 K). In order to replace Cd-based QDs, Cd-free  $\text{CuInS}_2/\text{ZnS}$  QDs incorporated with green  $\text{Eu}^{2+}:\text{BaSO}_4$  phosphor have been

prepared [35]. For fourth-generation development, the Illuminating Engineering Society of North America designed a new measurement module termed as TM-30-2015 having a defined color fidelity index (CFI, Rf) and color gamut index (CGI, Rg). In order to obtain an Rf value of over 90, it is difficult to produce warm-to-cool light W-LEDs. Warm-to-cool light W-LEDs should be produced for highly efficient white color. More recently, color-reproducible- and W-LEDs have been developed for next-generation lighting devices. The spectrum of QD-based W-LEDs should match daily fluctuation in sunlight under natural circadian rhythm for biological applications. The developed device is based on PQD having six-color white-light LEDs. In this module, six-colors, viz. cyan, green, yellowish green, amber, orange, and red of CsPbX<sub>3</sub> PQDs are used. The W-LED device thus packaged reveals high circadian with a tunable range and high color purity. The improved device shows a luminous efficiency (LE) of 58.8 lm w<sup>-1</sup>, a CRI value of 95, CFI with Rf = 91.4, and CGI with Rg = 102 and a CCT value of 6459 K. Circadian luminescence is established on the day-night rhythmic change of natural-light environments [36].

### 3.3 Phosphor-based LEDs

LEDs are most commonly referred to as a p-n junction diode that can emit visible radiation under the suitable current application to the leads (electrical connection connecting a length of wire/metal pad). The mechanism is based on the phenomenon of electroluminescence. In the electroluminescence process, the material emits light in response of electric current. **Figure 5(a)** and **(b)** represent electronic symbolic representation and packaged conventional LEDs, respectively. LEDs can be divided into two broad categories namely inorganic and organic LEDs (OLEDs). The OLEDs can further divide into two main groups: (1) small molecule OLEDs and (2) polymer OLEDs. Phosphor-based W-LEDs are main attraction due to their excellent properties such as low power consumption, long life, compactness, and environmental friendliness. The successful implementation for W-LEDs could be done via composed blue InGaN LED chip and phosphors (yellow emitting Y<sub>3</sub>Al<sub>5</sub>O<sub>12</sub>:Ce<sup>3+</sup> phosphor), and they are called phosphor converted W-LEDs [37].

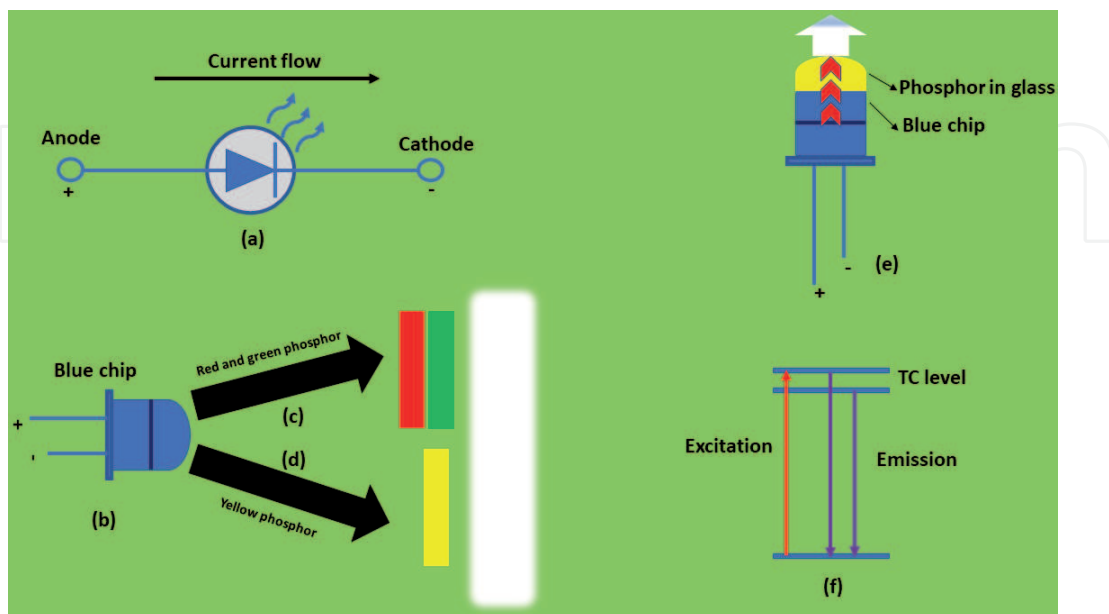


**Figure 5.** (a) Electronic symbolic representation, (b) packaged conventional blue LED chip, (c) white light generation from red and green phosphor, (d) white light generation from yellow phosphor, (e) white light emission from PIG operated with blue chip, and (f) excitation and emission process originated from the two TC energy levels.

The approaches for the generation of white light is based on the combination of two or more visible colors (mainly primary color red, green, and blue) emitting phosphor. The advantage of uses of blue LED chip is such that it can be used as excitation light to phosphors as well as a source of blue component. **Figure 5(c)–(e)** shows the white light generation from red and green phosphor, white light generation from yellow phosphor, and white light emission from phosphor in glass (PIG) operated with blue chip. There are some necessities in the LED phosphors for devices packaging, viz. high efficiency by blue light excitation, stability in harsh environment, low thermal quenching, and negligible deviation in emission spectrum (peak position and line width). **Table 3** shows some synthesized phosphor applicable in the W-LED application. RE-doped optical glasses are noncrystalline amorphous solid luminescent materials that can be utilized in the production of lenses, prism, optical window, and other optical components. RE-incorporated glasses also exhibit good luminescence that can be utilized in LED fabrication. PIG is considered to be a reasonable substitute that can overcome the luminescent degradation and color aberration issues. PIG has been recognized as a good material for high-power W-LED products for long-term service.

### 3.4 Optical temperature sensing

The noncontact optical temperature sensing can be realized by using the RE ion-doped phosphor due the presence of thermally coupled (TC) energy levels. These TC levels have been used in the measurement of fluorescence intensity ratio (FIR) investigation. The Boltzmann's distribution population law can be applied to measure the FIR under the application of the external temperature. The following Boltzmann's distribution population law can be used for FIR measurement:

$$\text{FIR} = \frac{I_u}{I_l} = B \exp(-\Delta E/kT) \quad (4)$$

where “ $I_u$ ” and “ $I_l$ ” are the integrated fluorescence intensities of the emissions from upper and lower TC energy level transitions, respectively. “ $B$ ” is the pre-exponential constant. “ $\Delta E$ ” is the energy gap of two TC energy levels. “ $k$ ” and “ $T$ ” are the Boltzmann's constant and absolute temperature, respectively. **Figure 5(f)** shows the excitation and emission process originated from the two TC energy levels. Sensor sensitivity ( $S$ ) of an optical sensing material is an important parameter and can be expressed as follows:

$$S = \frac{d(\text{FIR})}{dT} \quad (5)$$

where all the terms have their usual meaning. The FIR technique is suitably applied in the RE ion-doped material for the detection of the temperature. The method is also applicable for the measurement of optical heating for laser-based hyperthermia application.

### 3.5 Quantum dots for medical and clinical application

The developments of the QDs have shown a promising impact on the biological application due to their highly efficient emissive properties. It is believed that the bare (uncoated) QDs cannot be applied directly in biological application due to their inherent toxicity. Due to their toxic behavior, their implication in clinical usages is restricted. The QDs have proven their utility in bioapplications and are a better alternative of the traditional fluorophores. QDs possess a very good

Materials	Dopant ions	References
Y <sub>3</sub> Al <sub>5</sub> O <sub>12</sub>	Ce <sup>3+</sup>	[38]
Sr <sub>2</sub> B <sub>2</sub> O <sub>5</sub>	Tm <sup>3+</sup> , Na <sup>+</sup>	[39]
K <sub>3</sub> La(PO <sub>4</sub> ) <sub>2</sub>	Pr <sup>3+</sup>	[40]
Ba <sub>3</sub> GdNa(PO <sub>4</sub> ) <sub>3</sub> F	Eu <sup>2+</sup>	[41]
ZnWO <sub>4</sub>	Eu <sup>3+</sup> , Dy <sup>3+</sup>	[42]
Gd <sub>4</sub> O <sub>3</sub> F <sub>6</sub>	Er <sup>3+</sup> /Tm <sup>3+</sup> /Yb <sup>3+</sup>	[43]
LiNbO <sub>3</sub>	Ho <sup>3+</sup> /Yb <sup>3+</sup> /Tm <sup>3+</sup>	[44]

**Table 3.**  
 Some synthesized phosphor applicable in the W-LED application.

photostability, tunable emission, and longer lifetime. Currently, the major scope is to synthesize more biocompatible QDs in such a way that they can be used in terms of size, bio-conjugation, surface functionality, and targeting facilities. The nanotechnology related to life-science and bioscience is called “Nano biotechnology”. The nanobiotechnology is a very fast growing area and is a challenging task for the researchers working in this area. The remarkable result in the form of the useful medicine increases the attention in progress of novel therapy and diagnostic methods. The nanomaterials that preserve a broad scope in such novel areas are known as nanomedicines. Recently, the use of the QDs has been found to increase progressively in *in vitro* and *in vivo* based biomedical experiments. It is supposed that the QDs have specific properties such as adequate circulating lifetime and minimal nonspecific deposition and must retain their fluorescence for a satisfactorily long time.

The essentiality for the use of QDs in the surface passivated could be explained via three terms that are given as follows:

- i. Surface-based properties (effect on the fluorescence and emission mechanism): the fluorescence property in the nanocrystalline particles can be quenched in bare QDs due to the surface defect caused by high surface energy associated with the nanoparticles [45, 46]. The main drawback comes due to the surface oxidation in bare QDs, photo-degradation, and leaching of metal ions via long-term contact of QDs to ionic media/cellular media causing metal ion toxicity effect [47]. To reduce this effect, it is essential to cap the surface of the QDs via a suitable covering agent (ZnS, etc.).
- ii. Solubility: solubility is important for the effective optical property utilization of the QDs in the aqueous medium. The capping of the QDs provides an outer shell which improves the stability and reduces the solubility of the QDs in aqueous medium. The synthesis of QDs required a high temperature synthesis environment such as thermolysis, hot injection, and various other methods. Also, the size and agglomeration can be controlled via using the organic solvents (octane, hexane, trioctylphosphine oxide, octadecene, etc.) The stabilization can be achieved by using hydrophobic groups such as amines or phosphines. But the intrinsic solubility of these stabilized QDs is poor. To increase the solubility in the aqueous solution, coating of the QDs surface by hydrophilic ligand is important [48–50]. The hydrophilic ligand can be overcoated by using ligand exchange, surface silanization, and amphiphilic combination [50–52]. Medintz et al. have reported a detailed schematic of common QD solubilization and biofunctionalization [53].

Caps or ligand was used in biofunctionalization. Linkage to the QDs is given in pink color, biomolecule linking functionality is given in green color, and water solubility is given in blue color. Some models of the surface capping strategy and their interaction mechanism with the QDs and aqueous medium. For the cap exchange (top right) excess thiolated cap relocates the original TOP or TOPO coating via binding the ZnS surface layer with the thiol group and imparting hydrophilicity with the charged carboxyl (or other functionalities) which provides soluble colloidal QD dispersion.

- iii. Targeted delivery of QDs: for targeted drug delivery (for in-vitro and in-vivo) of the QDs, the choice of use of the abovementioned processes depends on the application and also on the easy availability to carry out the strategy. It is observed that many alternative methods/strategies and ligands have been prepared for the specific biological applications. The essential steps required for the target specific delivery of the QDs are to reduce their effect over the nonrelevant cells, increase greater contrast in the localized area, and utilize more effective FRET-based processes to get better results [54].

The modifications of the QD surface for the labeling of a target can be done by using antibodies or enzymes, small molecules, and peptides [55, 56]. The versatile strategy has been found to be useful by antibodies. The requirements of the synthetic procedures can be utilized in the small molecules, and hence, it is complicated. It is observed that each process has its own advantage and disadvantage and thus no unique approach was seen to be ubiquitous for all applications [55–57]. The cell culture examination observed in most of the cases of vitro cell culture cannot show complete vivo tissue system. In this, various interactions between cell to cell and/or cell to matrix and many other diffusion /transport situations take place. The existence of the cells in the body exhibits 3D environments and is very serious for their growth and metabolism [58]. In the case of 2D cell culture on a flat substrate, all these interactions are effectively reduced, and thus, it confines their capacity to reiterate the appropriate level of in-vivo cellular retorts [59].

Lee et al. [60] first time performed a 3D spheroid culture-based NP toxicity testing arrangement by using 3D-liver-tissue-spheroid models with human hepatocarcinoma (HepG2) cells. The human liver is considered as the main organ for NP gathering. The detailed investigation of the toxicity of cadmium telluride (CdTe) QDs in cell culture and in a 3D model has been signified. The model can be supposed to be intermediates between in vitro and in vivo observations. In the case of 2D cell culture, the HepG2 cells are attached closely to each other which exist in normally flat shape after spreading on a well-plate. On CdTe QD exposer, morphology was found to be changed after 12 h culture. A sufficient number of cells are disturbed (contracted and curved/roosted) and some are detached from the well-plate. The similar observation was observed in the case of CTAB-AuNPs in 2D cell culture. But, the negligible change in the cellular structure was seen in the citrate-stabilized gold (Au) NPs. Also, no significant morphology was changed in the 3D spheroid culture. However, a small rough spheroid surface in the CdTe and CTAB-Au NP-treated cultures was found. For the clear view, the confocal microscopy was used to identify the live or dead cells. It was observed that the dead cells (red in color) in 2D culture transferred into granular shape and were missing from the plate after dropping their cell-cell and cell-substrate interactions. Nevertheless, the spheroid culture has not changed any different morphology, and apparently, a small number of dead cells were found in the surface of the spheroids in a rugged manner. The observation tells that in the spheroid culture small dead cells are present as

compared to the 2D culture. This study suggests a comparative result between the 2D and 3D culture of HepG2 cells.

It is difficult to elucidate significant prediction by vivo effects based on the observation of vitro examination. The accurate mechanism involved in QD interaction with the body with metabolism distribution and final elimination after the uptake/delivery is still not cleared. Generally, NPs treated before the delivery follow long visit via altered body transport systems. Injection is considered as one of the main ways for QD-based vivo studies. The exogenous particle contains various serum proteins that can be carried out by blood. Protein corona formed by the interaction of the QD and protein can develop as a layer on the QD surface. Protein corona formed on the surface of the NPs affects biodistribution and biocompatibility. The available bloodstream helps in the delivery of NPs in various tissues and organs. The distribution is related to physio-anatomical structures of the vasculature and the physicochemical properties of the NPs. On completion of the distribution, the QDs undergo metabolic processing and will be evacuated from the body through the kidney and urine or feces. The excess sustained NPs inside of the body after holding long term periods can affect the normal function of organs/tissues. They can produce various toxicity levels such as metabolic toxicity, immunotoxicity, chronic organ toxicity, even genotoxicity, etc., [61]. The sufficient surface of vascular endothelial cells gives substantial space for the interactions with QDs specifically with negatively charged ones. The anionic QDs contain relatively low residence time in the blood and provide a huge accumulation in organs [62]. It has been observed that the high doses of the QDs produce contact activation and hence cause pulmonary vascular thrombosis by activating the coagulation cascade [63]. The importance of interaction of the QDs with blood cells is helpful in design for theranostic drug delivery resolutions. Fischer et al. have shown vivo mechanism by using two different (coated with mercaptoundecanoic acid and cross-linked with lysine and bovine serum albumin) coated QDs in rodents [64]. QDs coated with mercaptoundecanoic acid and cross-linked with lysine and bovine serum albumin was accumulated of about 40 and 99% in the liver after 90 min. A little amount of both the QDs was found in the spleen, kidney, and bone marrow. Moreover, the authors have not detected QDs in urine up to 10 days after intravenous dosing. Akerman et al. have observed a sufficient decrease of fluorescence via CdSe/ZnS QDs in animal studies using amphiphilic polymer and mercaptoacetic acid/peptide capped particles [65]. It has demonstrated slow metabolism degradation of QDs in mice. They observed a shift of the QD emission peak from red to blue upon long term exposure of over 2 years after injection of the QDs. In general, PEG-coated QDs decrease the toxicity in the cultured cells and provide good information related to lung tissue [66]. Tang et al. studied the biodistribution in mice and showed the effect of QD surface charge and their chemistry [67]. In spite of the surface chemistry and charge of the QDs, all the QDs produce toxic effect in liver, lung, and kidney after serious and long-term exposure. They observed that the PEG-coated QDs/negatively charged QDs accumulated in the liver. The positively charged QDs were located in the lung. The silica coted QDs after 5 days of injection show a very few of about 8.6% amount remaining in the hepatic tissue. But the QDs having approximate negligible protein corona were cleared through urine. The larger aggregated NPs can be transported to the liver and pass away via the bile excretion [68]. David Wegner and Hildebrandt have presented a broad review on different QD-based imaging applications for technological and the biological point of view [69]. Their review focused on the broad aspect of the QD utilization in in vivo and in vitro application extending from the super-resolution microscopy and single-particle tracking over in vitro cell and tissue imaging to in vivo examinations, drug or gene delivery to theranostic approaches and multimodal imaging.

Tsoi et al. have reported the blood clearance mechanism of managed hard nanomaterials or NPs relative to blood flow dynamics, organ microarchitecture, and cellular phenotype [70]. They observed that the velocity of the NPs which enters and traverse the liver reduces about 1000 times and shows 7.5 times NP interaction with the hepatic cells relative to peripheral cells. The three hard nanomaterial models, viz. quantum dots, gold nanoparticles, and silica nanoparticles, have been selected for the vivo examinations. **Figure 6** shows the distribution of QDs in the liver subsequent systemic intravascular injection. **Figure 6(a)** reflects the silver-stained section of a rat liver that was perfused 4 h post QDs injection. The accumulation of the QDs at a very higher amount was seen in the zone surrounding the portal triad than in the zone surrounding the central vein. Twenty-eight portal triad-central vein pairs have been analyzed. Here, one repeating unit of the liver microarchitecture is given for understanding **Figure 6(a)**. The blood flows can be seen from liver via the hepatic artery and portal vein that are positioned in the portal triad. The blood flows out of the liver through the central vein part of the liver. The zone of a radial distance of around 100  $\mu\text{m}$  was taken for the tracing for each vascular unit of the liver. In **Figure 6(a)**, the scale bar is taken as 100  $\mu\text{m}$ . The outline of the image processing that has been used to measure the accumulation of the QDs in the zone bordering of the portal triad and central vein has been shown in **Figure 6(b)**. Firstly, the zone surrounding each vascular structure has been removed by taking 100  $\mu\text{m}$  radius from the vessel border. Secondly, the images were converted into a binary format and thresholded to isolate

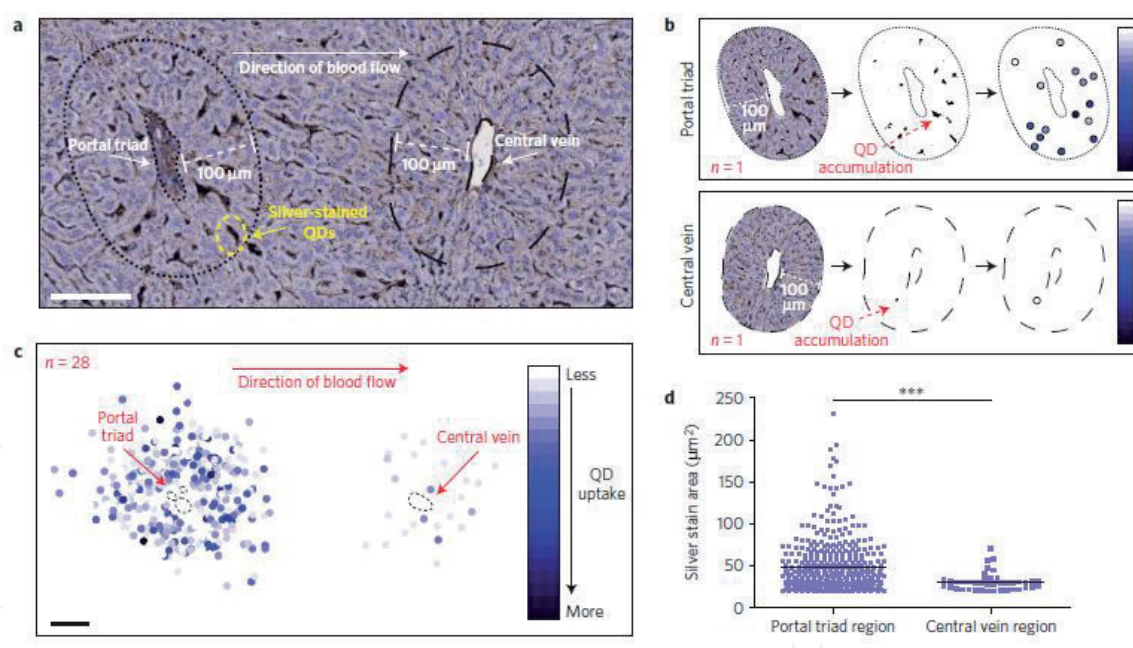


**Figure 6.**

*Distribution of the QDs in liver succeeding systemic intravascular injection. (a) Silver-stained segment of a rat-liver that is perfused 4-h post-QD-injection (counterstained with hematoxylin). One repeating unit of the liver microarchitecture has been shown. Blood is flowing into the liver through the hepatic artery and portal vein, which are positioned in the portal triad. Blood is flowing out of the liver via the central vein. A zone with a radial distance of 100  $\mu\text{m}$  was traced around each vascular unit. Scale bar is taken as 100  $\mu\text{m}$ . (b) An outline of the image processing used to quantify QD growth in the zones nearby the portal triad and central vein. First, the zone neighboring of each vascular construction was removed using a radius of 100  $\mu\text{m}$  from the vessel edge. Second, the image was transformed into a binary format and thresholded to isolate condensed silver. Finally, the area of each silver stain was controlled along with its coordinates (x, y) relative to the center of the vessel. The area of reduced silver corresponds to the amount of QDs gathering and is shown by a color range, where soft blue specifies a small amount of QD accumulation and dark blue shows a large amount of QDs gathering in each distinct position. (c) Twenty-eight portal triad-central vein pairs were analyzed and the results were combined. Scale bar is taken as 100  $\mu\text{m}$ . (d) Scatter plot associated with the area of each silver staining in the zone surrounding the portal triad versus in the zone surrounding the central vein. Here, the plotted data are displayed same as shown in (c). Statistical significance was assessed by using a two-tailed unpaired t-test. Reproduced with permission from Ref. [70].*

reduced silver. Then finally, the area of each silver strain has been scaled by using its coordinates  $(x, y)$  relative to the vessel center. The area of the QD accumulation has been given by a color spectrum in which the pale blue color represents a small amount of the QD accumulation and the dark blue reflects a large amount of QD accumulation in each individual location. The complete twenty-eight portal triad-central vein pairs were inspected. The combination of the results with the scale of the  $100 \mu\text{m}$  is shown in the **Figure 6(c)**. The area of each region of silver marking in the zone surrounding the portal triad versus in the zone surrounding the central vein has been illustrated in **Figure 6(d)**. The data points taken are the same as shown in **Figure 6(c)**. Moreover, two-tailed unpaired  $t$ -test was considered for the statistical significance of the data. The mechanism of nanomaterial transport in the liver has been shown in **Figure 7**. The NPs that are injected in the bloodstream encounter the mononuclear phagocyte system (MPS), which is the group of organs with containing phagocytic cells. The degree of NP uptake within each MPS organ can be monitored from the intensity of the blue color (see **Figure 7**). When the NPs transit from the peripheral circulation to the liver, the observed velocity is found to decrease up to 1000 folds. This implies that the NPs could interact with the liver and hence their clearance is possible from the bloodstream. There exist a concentration gradient in the NPs along the length of the sinusoid, and the amount of the NPs leaving the liver via the central vein is lower than the amount that enters through the portal triad.

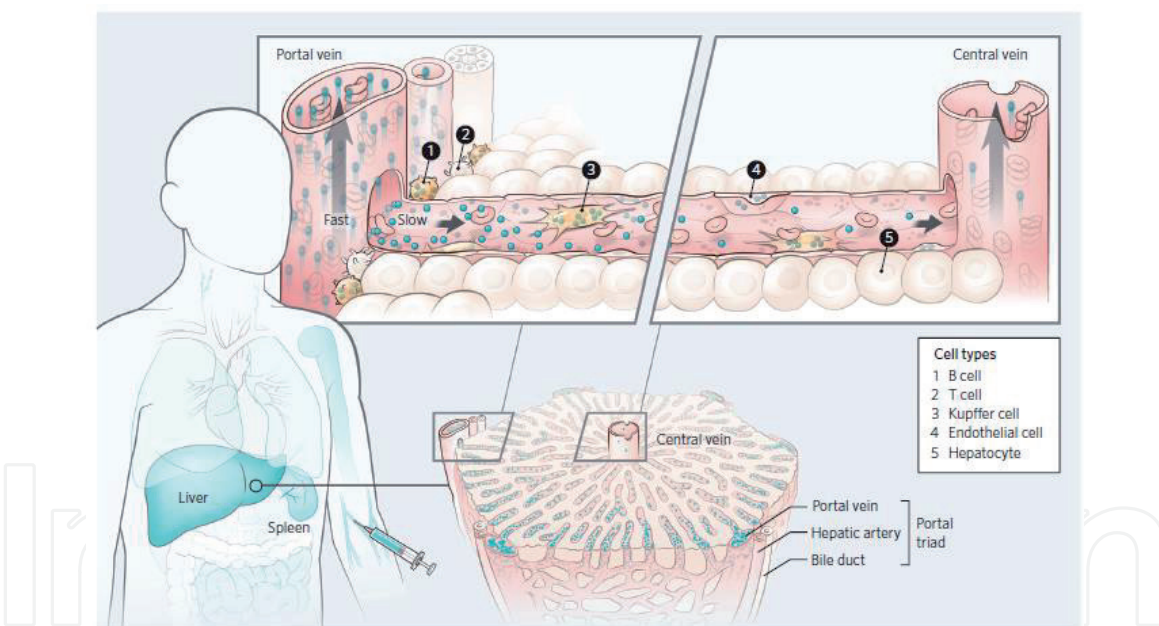


**Figure 7.**

*Nanomaterial or NP mechanism for the transportation in the liver. The injected NPs into the bloodstream meet the MPS, which is a group of organs containing phagocytic cells. The emission intensity of the blue color in the figure imitates the mark of nanomaterial/NPs uptake within each MPS organ. As the NPs' transition from the peripheral circulation to the liver takes place, 1000 times their velocity is found to reduce. This allows the NPs to interact with a variety of cells, hence resulting in their gradual clearance from the blood stream. A concentration gradient of nanomaterials/NPs along the length of the sinusoid is seen, and the amount leaving the liver through the central vein is lower than that of the amount which enters via the portal triad (see the diagram of liver lobule, as shown in the bottom right). The cells, "B" and "T" are showing a border to the portal triad and are exposed to a high concentration of incoming NPs (can be seen from the schematic of a liver sinusoid, top). The difference in nanomaterial/NP uptake between these two cell types is because of the increased endocytic/phagocytic capacity of "B" cells as compared with the "T" cells. From the NPs, that escaped the first set of cellular interactions which is moving along the sinusoid and can come into contact with endothelial and Kupffer cells. Hepatocytes are separated from the bloodstream by a layer of fenestrated endothelial cells and do not seem to take up intact with the hard nanomaterials/NPs. Nanomaterials/NPs that have been escaped uptake during a pass through the liver return to the systemic circulation via the central vein and are ultimately carried back to the liver (or another MPS organ). This process is repeated until nanomaterial/NP clearance from the bloodstream is completed. Reproduced with permission from Ref. [70].*

It can be seen that the “B” and “T” cells border the portal triad and open to a high concentration of incoming NPs. The observed differences that have been up-taken in both the NPs occur due to the increased endocytic or phagocytic capacity of “B” cells compared with “T” cells. The escaped NPs from the first set of cellular interaction can move along the sinusoid and hence can come into close contact with the endothelial and Kupffer cells. By a layer of fenestrated endothelial cells, the hepatocytes can be separated from the bloodstream and were not observed to take up hard NPs. The escaped NPs pass from the liver to the circulation process in the central vein and can return back to the liver or through the MPS organs. The steps involved in the process can be repeated by the NPs until the clearance from the blood stream is completed.

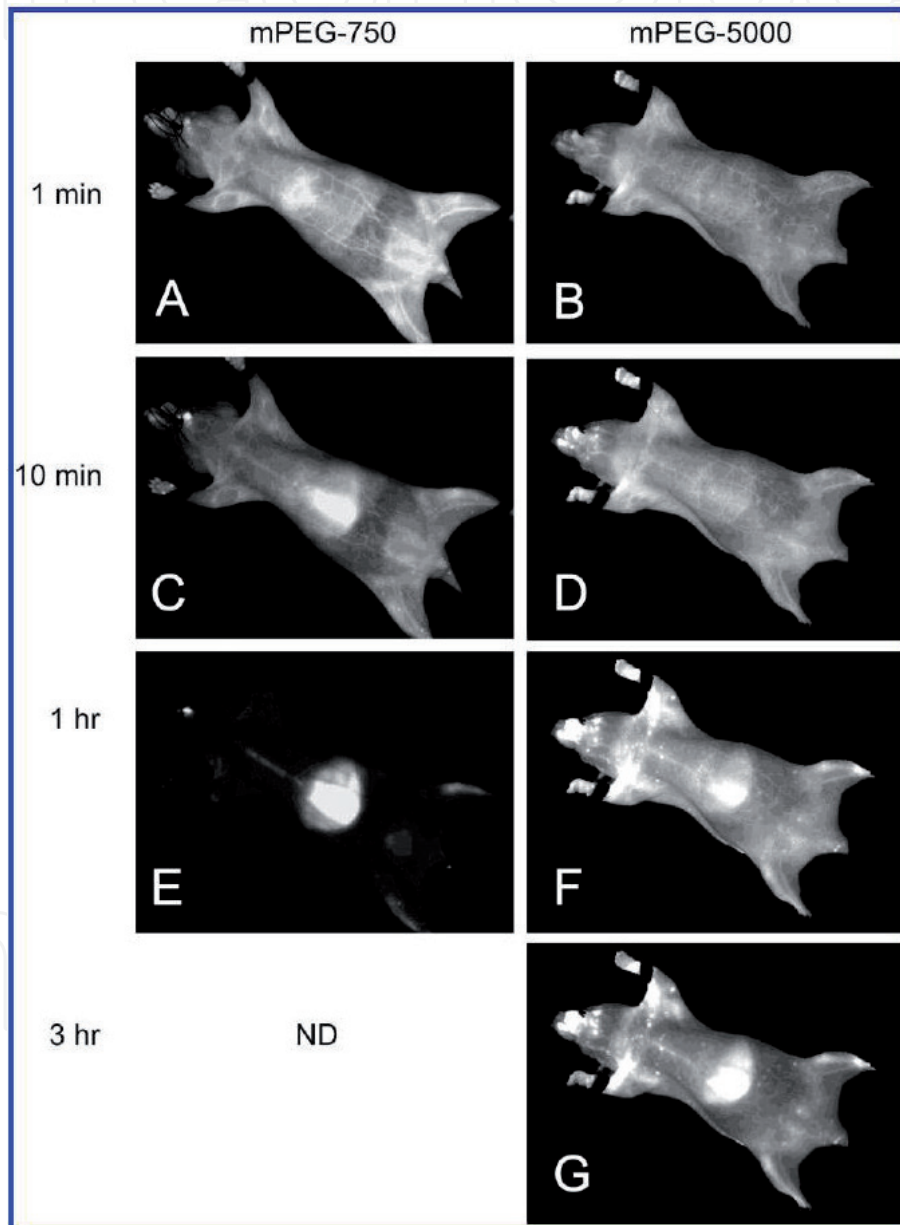


**Figure 8.**

Noninvasive imaging using 645 nm mPEG-750 QDs [left, (A, C, E)] and 655 nm-emitting mPEG-5000 QDs [right, (B, D, F, G)]. Nude mice have been taken to image at 1 min (A and B), 10 min (C and D), 1 h (E and F), and 3 h (G) post injection. It has been noted that even at 1 min, significant liver uptake is visible using mPEG-750 QDs (A), while even at 10 min there is little or no visible liver uptake using mPEG-5000 QDs (D). At 1 h, the difference between mPEG-750 QDs (E) and mPEG-5000 QDs is even more marked, with PEG-750 QDs completely cleared from the circulation, while mPEG-5000 QDs persist (F); even 3 h post injection, mPEG-5000 QDs remain in circulation (G). Since it is essentially found that all fluorescence was cleared from the circulation by 1 h, imaging of mPEG-750 QDs was terminated at 1 h after injection. In other experiments, we found that the pattern of deposition of mPEG-750 QDs can be seen at 1 h which remained stable for at least 24 h. Reproduced with permission from Ref. [71].

Ballou et al. have tested four different surface-coated QDs in *in vivo* imaging [71]. They have shown the QD localization using fluorescence imaging of living animals by necropsy, electron microscopy, frozen tissue sections (optical microscopy), and on scales oscillating from centimeters to nanometers for detection purpose by using only QDs. **Figure 8** shows the noninvasive imaging using 645 nm methoxy- or carboxy-terminated poly(ethylene glycol) amine, that is, mPEG-750 QDs (left, A, C, E) and 655 nm-emitting mPEG-5000 QDs (right, B, D, F, G). Nude mice were taken for the imaging at various time scales, 1 min, 10 min, 1 h, and 3 h, post injection for the study. It has been noted that even at 1 min, sufficient liver uptake is found to be visible by using mPEG-750 QDs (A); after 10 min only a very little or negligible visible liver uptake using mPEG-5000 QDs (D) was found. At 1 h time, an important difference between mPEG-750 QDs (E) and mPEG-5000 QDs is to be remarked, with PEG-750 QDs completely cleared from the circulation process, while mPEG-5000 QDs are to be seen persevered; even 3 h post injection, mPEG-5000 QDs remain in circulation. Moreover, it is crucial that all fluorescence is cleared from the circulation by up to 1 h; imaging of mPEG-750 QDs was found to complete at 1 h after injection. In other trials, they observed that the pattern of deposition of mPEG-750 QDs was realized at 1 h, which remained stable for at least 24 h.

The small QDs can penetrate in the blood-vessel walls and tissues and work as tracing peptides, in the *in vivo* antibody, tumor targeting, and as lymph node mapping due to their penetration of lymphatic walls [72–74]. But, the ability of the QDs to penetrate in other immunological barriers is not very much clear to date. Placental barrier (acts as a discriminating membrane to substances passing from maternal to fetal blood) has been considered an important process in humans/animals because of the prevention from the foreign materials via bacteria, viruses, and other organic or inorganic particles. Moreover, all foreign materials cannot effectively stop by this barrier. Some drugs cannot be employed in pregnant woman since it can be transported to the fetus across the placental barrier. At that place, they have the possibility to cause congenital malformations or miscarriage [75]. Chu et al. have reported [76] the inspection of intact QDs within the placental barrier. The transfer of QDs from pregnant animals to fetuses was reported successfully. The fetuses were cryosectioned at the time of observation. The ultrafine sections were distinguished with the support of fluorescence microscopy. Fluorescence was not at all observed in any tissues from QDs (red in color). The findings suggest that the QDs may be passed from female mice to their fetuses across the placental barrier. The small QDs have been transferred easily than their larger counterpart. The number of the QDs thus transferred will turn on the dosage. The increase in the QD dosage reveals enhancement in the transportation. Moreover, the QDs coated with the silica or other organic (such as polyethylene glycol PEG) layer could hinder the transportation process. This result shows that the clinical approach of QDs is limited in pregnant women.

#### 4. Conclusion

The chapter includes a verity of luminescent materials that are useful in diverse applications such as development of the LEDs, display, temperature sensing, and biomedical applications. The spectroscopy of rare earth ions with their basic properties has been given in detail. The mechanism for understanding the emission processes involved in the RE activated optical materials has been discussed in a broad view by taking the concept of energy migration within the luminescent ions. The uses of these optical materials, viz. quantum dots and phosphors, have been incorporated. A broad view of the quantum dots has been accounted while considering the surface modification to show their biomedical application.

## **Acknowledgements**

Abhishek Kumar Soni acknowledges the award of National Post-Doctoral Fellowship provided by the Science and Engineering Research Board (SERB), Government of India through N-PDF file No. PDF/2016/003419. Bheeshma Pratap Singh acknowledges the Department of Science and Technology (DST), New Delhi, India, through its DST-INSPIRE Faculty Award (IFA-17 MS-109) program.

IntechOpen

IntechOpen

### **Author details**

Abhishek Kumar Soni\* and Bheeshma Pratap Singh\*  
Chemistry Division, Bhabha Atomic Research Centre, Mumbai, India

\*Address all correspondence to: aksoni.ism@gmail.com and  
bheeshmapratap@gmail.com

### **IntechOpen**

---

© 2019 The Author(s). Licensee IntechOpen. This chapter is distributed under the terms of the Creative Commons Attribution License (<http://creativecommons.org/licenses/by/3.0>), which permits unrestricted use, distribution, and reproduction in any medium, provided the original work is properly cited. 

## References

- [1] Feldmann C, Justel T, Ronda CR, Schmidt PJ. Inorganic luminescent materials: 100 years of research and application. *Advanced Functional Materials*. 2003;**13**:511-516
- [2] Blasse G, Grabmaier BC. *Luminescent Materials*. Berlin: Springer; 1994
- [3] Ronda CR. In: Ronda CR, editor. *Luminescence from Theory to Applications*. Weinheim: Wiley-VCH Verlag GmbH & Co. KGaA; 2008. pp. 1-34
- [4] Bhargava RN, Gallagher D, Hong X, Nurmikko A. Optical properties of manganese-doped nanocrystals of ZnS. *Physical Review Letters*. 1994;**72**:416
- [5] Miniscalco WJ. *Optical and Electronic Properties of Rare Earth Ions in Glasses*. Optical Engineering. New York: Marcel Dekker Incorporated; 2001. pp. 17-112
- [6] van Dijk JMF, Schuurmans MFH. On the nonradiative and radiative decay rates and a modified exponential energy gap law for  $4f-4f$  transitions in rare-earth ions. *The Journal of Chemical Physics*. 1983;**78**:5317
- [7] Richards BS. Luminescent layers for enhanced silicon solar cell performance: Down-conversion. *Solar Energy Materials & Solar Cells*. 2006;**90**:1189
- [8] Auzel F. Upconversion and anti-stokes processes with f and d ions in solids. *Chemical Reviews*. 2004;**104**:139-174
- [9] Richards BS. Enhancing the performance of silicon solar cells via the application of passive luminescence conversion layers. *Solar Energy Materials & Solar Cells*. 2006;**90**:2329-2337
- [10] Huang X, Han S, Huang W, Liu X. Enhancing solar cell efficiency: The search for luminescent materials as spectral converters. *Chemical Society Reviews*. 2013;**42**:173
- [11] Boyer JC, van Veggel FCJM. Absolute quantum yield measurements of colloidal  $\text{NaYF}_4:\text{Er}^{3+}, \text{Yb}^{3+}$  upconverting nanoparticles. *Nanoscale*. 2010;**2**:1417
- [12] Zhang W, Ding F, Chou SY. Large enhancement of upconversion luminescence of  $\text{NaYF}_4:\text{Yb}^{3+}/\text{Er}^{3+}$  nanocrystal by 3D plasmonic nano-antennas. *Advanced Materials*. 2012;**24**:OP236
- [13] Huang XY, Zhang QY. Near-infrared quantum cutting via cooperative energy transfer in  $\text{Gd}_2\text{O}_3:\text{Bi}^{3+}, \text{Yb}^{3+}$  phosphors. *Journal of Applied Physics*. 2010;**107**:063505
- [14] Rakov N, Maciel GS. Near-infrared quantum cutting in  $\text{Ce}^{3+}, \text{Er}^{3+}$ , and  $\text{Yb}^{3+}$  doped yttrium silicate powders prepared by combustion synthesis. *Journal of Applied Physics*. 2011;**110**:083519
- [15] Zhou J, Zhuang Y, Ye S, Teng Y, Lin G, Zhu B, et al. Broadband downconversion based infrared quantum cutting by cooperative energy transfer from  $\text{Eu}^{2+}$  to  $\text{Yb}^{3+}$  in glasses. *Applied Physics Letters*. 2009;**95**:141101
- [16] Fan B, Chlique C, Conanec OM, Zhang X, Fan X. Near-infrared quantum cutting material  $\text{Er}^{3+}/\text{Yb}^{3+}$  doped  $\text{La}_2\text{O}_2\text{S}$  with an external quantum yield higher than 100%. *Journal of Physical Chemistry C*. 2012;**116**:11652
- [17] Butkus J, Vashishtha P, Chen K, Gallaher JK, Prasad SKK, Metin DZ, et al. The evolution of quantum confinement in  $\text{CsPbBr}_3$  perovskite nanocrystals. *Chemistry of Materials*. 2017;**29**:3644
- [18] Kim G-H, García de Arquer FP, Yoon YJ, Lan X, Liu M, Voznyy O, et al. High-efficiency colloidal quantum dot

- photovoltaics via robust self-assembled monolayers. *Nano Letters*. 2015;**15**:7691
- [19] Hoogland S, Sukhovatkin V, Howard I, Cauchi S, Levina L, Sargent EH. A solution-processed 1.53  $\mu\text{m}$  quantum dot laser with temperature-invariant emission wavelength. *Optics Express*. 2006;**14**:3273
- [20] Caruge JM, Halpert JE, Wood V, Bulovic V, Bawendi MG. Colloidal quantum-dot light-emitting diodes with metal-oxide charge transport layers. *Nature Photonics*. 2008;**2**:247
- [21] Chen CW, Wu DY, Chan YC, Lin CC, Chung PH, Hsiao M, et al. Evaluations of the chemical stability and cytotoxicity of  $\text{CuInS}_2$  and  $\text{CuInS}_2/\text{ZnS}$  core/shell quantum dots. *Journal of Physical Chemistry C*. 2015;**119**:2852
- [22] Nan W, Niu Y, Qin H, Cui F, Yang Y, Lai R, et al. Crystal structure control of zinc-blende  $\text{CdSe}/\text{CdS}$  core/shell nanocrystals: Synthesis and structure-dependent optical properties. *Journal of the American Chemical Society*. 2012;**134**:19685
- [23] Wu T, He K, Zhan Q, Ang S, Ying J, Zhang S, et al. MPA-capped  $\text{CdTe}$  quantum dots exposure causes neurotoxic effects in nematode *Caenorhabditis elegans* by affecting the transporters and receptors of glutamate, serotonin and dopamine at the genetic level, or by increasing ROS, or both. *Nanoscale*. 2015;**7**:20460
- [24] Moreels I, Justo Y, De Geyter B, Haustraete K, Martins JC, Hens Z. Size-tunable, bright, and stable  $\text{PbS}$  quantum dots: A surface chemistry study. *ACS Nano*. 2011;**5**:2004
- [25] Schmidt LC, Pertegás A, GonzálezCarrero S, Malinkiewicz O, Agouram S, Mínguez Espallargas G, et al. Nontemplate synthesis of  $\text{CH}_3\text{NH}_3\text{PbBr}_3$  perovskite nanoparticles. *Journal of the American Chemical Society*. 2014;**136**:850
- [26] Protesescu L, Yakunin S, Bodnarchuk MI, Krieg F, Caputo R, Hendon CH, et al. Nanocrystals of cesium lead halide perovskites ( $\text{CsPbX}_3$ , X = Cl, Br, and I): Novel optoelectronic materials showing bright emission with wide color gamut. *Nano Letters*. 2015;**15**:3692
- [27] Shimizu KT, Böhmer M, Estrada D, Gangwal S, Grabowski S, Bechtel H, et al. Toward commercial realization of quantum dot based white light-emitting diodes for general illumination. *Photonics Research*. 2017;**5**:A1
- [28] Jang E, Jun S, Jang H, Lim J, Kim B, Kim Y. White-light-emitting diodes with quantum dot color converters for display backlights. *Advanced Materials*. 2010;**22**:3076
- [29] Dai X, Zhang Z, Jin Y, Niu Y, Cao H, Liang X, et al. Solution-processed, high-performance light-emitting diodes based on quantum dots. *Nature*. 2014;**515**:96
- [30] Yoon HC, Oh JH, Lee S, Park JB, Do YR. Circadian-tunable perovskite quantum dot-based down-converted multi-package white LED with a color fidelity index over 90. *Scientific Reports*. 2017;**7**:2808
- [31] Lin CC, Liu RS. Advances in phosphors for light-emitting diodes. *Journal of Physical Chemistry Letters*. 2011;**2**:1268
- [32] Wang B, Lin H, Xu J, Chen H, Wang Y.  $\text{CaMg}_2\text{Al}_6\text{O}_{27}:\text{Mn}^{4+}$ -based red phosphor: A potential color converter for high-powered warm W-LED. *ACS Applied Materials & Interfaces*. 2014;**6**:22905
- [33] Zhu H, Lin CC, Luo W, Shu S, Liu Z, Liu Y, et al. Highly efficient non-rare-earth red emitting phosphor for warm white light-emitting diodes. *Nature Communications*. 2014;**5**:4312

- [34] Wang X, Yan X, Li W, Sun K. Doped quantum dots for white-light-emitting diodes without reabsorption of multiphase phosphors. *Advanced Materials*. 2012;**24**:2742
- [35] Chuang PH, Lin CC, Liu R-S. Emission-tunable CuInS<sub>2</sub>/ZnS quantum dots: Structure, optical properties, and application in white light-emitting diodes with high color rendering index. *ACS Applied Materials & Interfaces*. 2014;**6**:15379
- [36] Wang HC, Bao Z, Tsai HY, Tang AC, Liu RS. Perovskite quantum dots and their application in light-emitting diodes. *Small*. 2017;**14**:1702433
- [37] Soni AK, Mahata MK. Photoluminescence and cathodoluminescence studies of Er<sup>3+</sup>-activated strontium molybdate for solid-state lighting and display applications. *Materials Research Express*. 2017;**4**:126201
- [38] Niu X, Xun J, Prog ZY. The spectroscopic properties of Dy<sup>3+</sup> and Eu<sup>3+</sup> co-doped Y<sub>3</sub>Al<sub>5</sub>O<sub>12</sub> (YAG) phosphors for white LED. *Natural Science*. 2015;**25**:209
- [39] Cai L, Ying L, Zheng J, Fan B, Chen R, Chen C. Luminescent properties of Sr<sub>2</sub>B<sub>2</sub>O<sub>5</sub>: Tm<sup>3+</sup>, Na<sup>+</sup> blue phosphor. *Ceramics International*. 2014;**40**:6913
- [40] Bedyal AK, Ramteke DD, Kumar V, Swart HC. Blue photons excited highly chromatic red light emitting K<sub>3</sub>La(PO<sub>4</sub>)<sub>2</sub>:Pr<sup>3+</sup> phosphors for white light emitting diodes. *Materials Research Bulletin*. 2018;**103**:173
- [41] Li C, Dai J, Huang J, Deng D, Yu H, Wang L, et al. Crystal structure, luminescent properties and white light emitting diode application of Ba<sub>3</sub>GdNa(PO<sub>4</sub>)<sub>3</sub>F:Eu<sup>2+</sup> single-phase white light-emitting phosphor. *Ceramics International*. 2016;**42**:6891
- [42] Zhai Y, Wang M, Zhao Q, Yu J, Li X. Fabrication and luminescent properties of ZnWO<sub>4</sub>:Eu<sup>3+</sup>, Dy<sup>3+</sup> white light-emitting phosphors. *Journal of Luminescence*. 2016;**172**:161
- [43] Passuello T, Piccinelli F, Pedroni M, Bettinelli M, Mangiarini M, Naccache R, et al. White light upconversion of nanocrystalline Er/Tm/Yb doped tetragonal Gd<sub>4</sub>O<sub>3</sub>F<sub>6</sub>. *Optical Materials*. 2011;**33**:643
- [44] Xing L, Wang R, Xu W, Qian Y, Xu Y, Yang C, et al. Upconversion white-light emission in Ho<sup>3+</sup>/Yb<sup>3+</sup>/Tm<sup>3+</sup> codoped LiNbO<sub>3</sub> polycrystals. *Journal of Luminescence*. 2012;**132**:1568
- [45] Manna L, Scher EC, Li LS, Alivisatos AP. Epitaxial growth and photochemical annealing of graded CdS/ZnS shells on colloidal CdSe nanorods. *Journal of the American Chemical Society*. 2002;**124**:7136
- [46] Hess BC, Okhrimenko IG, Davis RC, Stevens BC, Schulzke QA, Wright KC. Surface transformation and photoinduced recovery in CdSe nanocrystals. *Physical Review Letters*. 2001;**86**:3132
- [47] Singh S, Sharma A, Robertson GP. Realizing the clinical potential of cancer nanotechnology by minimizing toxicologic and targeted delivery concerns. *Cancer Research*. 2012;**72**:5663
- [48] Gao X, Cui Y, Levenson RM, Chung LW, Nie S. In vivo cancer targeting and imaging with semiconductor quantum dots. *Nature Biotechnology*. 2004;**22**:969
- [49] Kairdolf BA, Mancini MC, Smith AM, Nie S. Minimizing nonspecific cellular binding of quantum dots with hydroxyl-derivatized surface coatings. *Analytical Chemistry*. 2008;**80**:3029
- [50] Thanha NTK, Green LAW. Functionalisation of nanoparticles for

- biomedical applications. *Nano Today*. 2010;**5**:213
- [51] Li H, Shih WY, Shih WH. Highly photoluminescent and stable aqueous ZnS quantum dots. *Industrial and Engineering Chemistry Research*. 2010;**49**:579
- [52] Lukehart CM, Scott RA, editors. *Nanomaterial Inorganic and Bioinorganic Perspective*. John Wiley & Sons; 2013. pp. 512-513. Available from: <https://www.wiley.com/en-us/Nanomaterials%3A+Inorganic+and+Bioinorganic+Perspectives-p-9780470516447>
- [53] Medintz IL, Uyeda HT, Goldman ER, Mattoussi H. Quantum dot bioconjugates for imaging, labelling and sensing. *Nature Materials*. 2005;**4**:435
- [54] Jamieson T, Bakhshi R, Petrova D, Pocock R, Imani M, Seifalian AM. Biological applications of quantum dots. *Biomaterials*. 2007;**28**:4717
- [55] Rosenthal SJ, Chang JC, Kovtun O, McBride JR, Tomlinson ID. Biocompatible quantum dots for biological applications. *Chemistry & Biology*. 2011;**18**:10-24
- [56] Goldman ER, Anderson GP, Tran PT, Mattoussi H, Charles PT, Mauro JM. Conjugation of luminescent quantum dots with antibodies using an engineered adaptor protein to provide new reagents for fluoroimmunoassays. *Analytical Chemistry*. 2002;**74**:841
- [57] Chana WCW, Maxwell DJ, Gao X, Bailey RE, Han M, Nie S. Luminescent quantum dots for multiplexed biological detection and imaging. *Current Opinion in Biotechnology*. 2002;**13**:40
- [58] Gartner PL, Hiatt LJ. *Color Text Book of Histology*. Philadelphia, PA: Saunder; 2001
- [59] Lee J, Cuddihy MJ, Kotov NA. Three-dimensional cell culture matrices: State of the art. *Tissue Engineering Part B*. 2008;**14**:61
- [60] Lee J, Lilly GD, Doty RC, Podsiadlo P, Kotov NA. In vitro toxicity testing of nanoparticles in 3D cell culture. *Small*. 2009;**5**:1213
- [61] Li J, Chang X, Chen X, Gu Z, Zhao F, Chai Z, et al. Toxicity of inorganic nanomaterials in biomedical imaging. *Biotechnology Advances*. 2014;**32**:727
- [62] Praetner M, Rehberg M, Bihari P, Lerchenberger M, Uhl B, Holzer M, et al. The contribution of the capillary endothelium to blood clearance and tissue deposition of anionic quantum dots in vivo. *Biomaterials*. 2010;**31**:6692
- [63] Geys J, Nemmar A, Verbeken E, Smolders E, Ratoi M, Hoylaerts MF, et al. Acute toxicity and prothrombotic effects of quantum dots: Impact of surface charge. *Environmental Health Perspectives*. 2008;**116**:1607
- [64] Fischer HC, Liu L, Pang KS, Chan WCW. Pharmacokinetics of nanoscale quantum dots: In vivo distribution, sequestration, and clearance in the rat. *Advanced Functional Materials*. 2006;**16**:1299
- [65] Akerman ME, Chan WCW, Laakkonen P, Bhatia SN, Ruoslahti E. *Proceedings of the National Academy of Sciences of the United States of America*. 2002;**99**:12617
- [66] Ho C-C, Chang H, Tsai H-T, Tsai M-H, Yang C-S, Ling Y-C, et al. Quantum dot 705, a cadmium-based nanoparticle, induces persistent inflammation and granuloma formation in the mouse lung. *Nanotoxicology*. 2013;**7**:105
- [67] Tang Y, Han S, Liu H, Chen X, Huang L, Li X, et al. The role of surface chemistry in determining in vivo biodistribution and toxicity of CdSe/ZnS core-shell quantum dots. *Biomaterials*. 2013;**34**:8741

- [68] Chen Z, Chen H, Meng H, Xing G, Gao X, Sun B, et al. Bio-distribution and metabolic paths of silica coated CdSeS quantum dots. *Toxicology and Applied Pharmacology*. 2008;**230**:364
- [69] David Wegner K, Hildebrandt N. Quantum dots: bright and versatile in vitro and in vivo fluorescence imaging biosensors. *Chemical Society Reviews*. 2015;**44**:4792
- [70] Tsoi KM, MacParland SA, Ma XZ, Spetzler VN, Echeverri J, Ouyang B, et al. Mechanism of hard-nanomaterial clearance by the liver. *Nature Materials*. 2016;**15**:1212
- [71] Ballou B, Lagerholm BC, Ernst LA, Bruchez MP, Waggoner AS. Noninvasive imaging of quantum dots in mice. *Bioconjugate Chemistry*. 2004;**15**:79
- [72] Cai W, Shin D-W, Chen K, Gheysens O, Cao Q, Wang SX, et al. Peptide-labeled near-infrared quantum dots for imaging tumor vasculature in living subjects. *Nano Letters*. 2006;**6**:669
- [73] Kerman M, Chan WCW, Laakkonen P, et al. Nanocrystal targeting in vivo. *PNAS*. 2002;**99**:12617
- [74] Kim S, Lim YT, Soltesz EG, Grand AMD, Lee J, Nakayama A, et al. Near-infrared fluorescent type II quantum dots for sentinel lymph node mapping. *Nature Biotechnology*. 2004;**22**:93
- [75] Briggs GG, Freeman RK, Yaffe SJ. *Drugs in Pregnancy and Lactation: A Reference Guide to Fetal and Neonatal Risk*. Lippincott Williams & Wilkins; 2012. Available from: <https://books.google.co.in/books?hl=hi&lr=&id=ScPvM03B3lUC&oi=fnd&pg=PA181&dq=Briggs+GG,+Freeman+RK,+Yaffe+SJ,+Drugs+in+Pregnancy+and+Lactation,+Lippincott+Williams+%26+Wilkins%3B+2001&ots=tJT5pDgZrj&sig=xocU0n9TwtWdK6WLCuOVnxz0tjc#v=onepage&q&f=false>